Electromagnetic excitation of phonons at C(001) surfaces

2009 J. Phys.: Condens. Matter 21 355010

(http://iopscience.iop.org/0953-8984/21/35/355010)

J. Phys.: Condens. Matter **21** (2009) 355010 (9pp) doi:10.1088/0953-8984/21/35/355010

Electromagnetic excitation of phonons at C(001) surfaces

F L Pérez-Sánchez[1] **and F Pérez-Rodríguez**[2]

[1] Escuela de Ciencias, Universidad Autónoma 'Benito Juárez' de Oaxaca, Avenida Universidad S/N, Ex-Hacienda de Cinco Señores, Ciudad Universitaria, Oaxaca de Juárez, Oaxaca, 68120, Mexico
[2] Instituto de Física, Benemérita Universidad Autónoma de Puebla, Apartado Post. J-48, Puebla 72570, Mexico

E-mail: fperez@sirio.ifuap.buap.mx

Received 30 March 2009, in final form 22 July 2009
Published 10 August 2009
Online at stacks.iop.org/JPhysCM/21/355010

Abstract
The photon–phonon coupling at C(001)-(2 × 1) surfaces and its manifestation in far-infrared reflectance anisotropy spectra (FIR-RAS) are theoretically investigated. We solve the coupled system of equations for the electromagnetic field and lattice vibrations, described within the adiabatic bond charge model (ABCM), with the method of expansion into bulk phonon and photon modes. The calculated FIR-RAS exhibit resonances associated with zone-center surface phonons in good agreement with available HREELS experiments and predictions of vibrational modes for diamond (001)-(2 × 1) surfaces from ABCM and *ab initio* calculations. Interestingly, the reflectance anisotropy spectra for a C(001)-(2 × 1) surface turn out to be qualitatively different from the spectra for a Si(001)-(2 × 1) surface, reported previously.

1. Introduction

During the past few decades, surface phonons have been intensively investigated (see, for example [1–6], and references cited therein). Their frequencies can be measured by means of helium atom scattering (HAS) [3] and high-resolution electron energy loss spectroscopy (HREELS) [1, 7, 8]. Optical spectroscopies (for example, infrared (IR) absorption [9, 10], IR ellipsometry [11], IR attenuated total reflection [12, 13], Raman scattering [14, 15], and sum-frequency generation [16, 17]) are also employed in investigating the motion of surface atoms and have the advantage, in comparison with HAS and HREELS, that they do not damage the sample and do not require an ultra-high vacuum. Therefore, optical spectroscopies can be applied to study surfaces of samples embedded in a gas or a liquid.

Another optical spectroscopy used for investigating surface phonons is reflectance anisotropy spectroscopy (RAS) [18]. RAS, which is also known as reflectance difference spectroscopy (RDS), is a linear optical technique based on the measurement of the difference between the normal-incidence optical reflectance of light polarized along two mutually perpendicular directions on the surface plane as a function of the photon energy [19–21]. In a cubic crystal, whose optical properties in the bulk are isotropic, the anisotropy observed by means of RAS must be associated with the reduced symmetry on the surface. RAS has been successfully applied in the visible and ultraviolet spectral ranges for investigating electronic, structural, and chemical properties of surfaces (see, for example [22–29]).

The application of RAS in the far infrared for studying the electromagnetic excitation of vibrational surface modes was first discussed in [18]. There, it was demonstrated that the reflectivity spectrum shows deviations from the spectrum calculated by using the Fresnel formulae of the order of 10^{-4}–10^{-3} because of the coupling of photons with surface phonons. These small deviations can be observed in the spectra of RAS. Due to the fact that the wavevector q of the incident light is rather small in comparison with the inverse of the lattice constant a ($qa \ll 1$), reflectance anisotropy spectroscopy in the far infrared (FIR-RAS) can be applied for investigating the excitation of surface vibrational modes near the center of the bidimensional Brillouin zone (i.e. near $\bar{\Gamma}$ point). However, if the surface is reconstructed, FIR-RAS might allow us to detect excited modes at other points of the 2D Brillouin zone. Because of the sensitivity of RAS to surface phonons, it can be used as a complementary technique to infrared spectroscopies, having a prominent bulk signal that might obstruct the detection of surface vibrational modes.

The first spectra of far-infrared reflectance anisotropy were calculated for ideal nonreconstructed (110) surfaces of

zinc-blende semiconductors [18, 30]. In the calculations, a microscopic formalism based on the Born model [31], including Coulomb interactions and retarded interactions, was employed to describe the interactions between atoms in a semi-infinite crystal. Despite its simplicity, such a formalism showed that FIR-RAS spectra exhibit resonances associated with surface phonons [18, 30]. The description of the interaction between ions in zinc-blende crystals was improved in [32] by using the model of valence force potentials proposed by Keating [33]. The reflectivity spectra for nonreconstructed (001) surfaces of GaAs and InP calculated in [32] present a resonance structure that is sensitive to the orientation of the polarization of the incident light with respect to the principal axes of the crystal surface. The resonances appearing in the gap limited by the acoustic and optical transverse branches were associated with microscopic Lucas modes, which are excited well when the lighter atoms are at the crystal surface.

In our previous work [34], the coupling of surface phonons with light at Si(001) surfaces in the asymmetric (2×1) dimer geometry, and its manifestation in far-infrared reflectance anisotropy spectra were investigated. There, we have applied the adiabatic bond charge model (ABCM) [35, 36] to describe short-range mechanical interactions together with long-range Coulomb forces and radiation fields. The use of the ABCM is advantageous since it is possible to study the photon–phonon coupling at surfaces of homopolar semiconductors. It should be mentioned that the resonances in the reflectance anisotropy spectra, predicted in [34], were clearly identified by comparison with the surface phonon frequencies of Si(001)-(2×1) at the $\bar{\Gamma}$ point, which had been calculated in [37] with the same ABCM.

In this paper, we shall investigate the photon–phonon coupling at C(001)-(2×1) surfaces in order to determine the infrared-active surface phonons that can be detected by FIR-RAS. Such a reconstructed surface is characterized by a symmetric dimer [38–42], and has been studied by employing RAS in the visible and ultraviolet frequency ranges [43–46]. It is interesting that the optical spectra for the C(001)-(2×1) surface exhibit a different anisotropy in comparison with the Si(001)-(2×1). The reason for such a difference is due to the dimer buckling that occurs at the Si(001)-(2×1) surface, but not at the C(001)-(2×1) surface [39, 45, 46]. As is already known (see, for example, [39, 4]), the rebuilding of the dimer observed in Si(001), but not in C(001), is due to the fact that $p(s)$ valence orbitals are more extended than $s(p)$ valence orbitals for Si (C). In the case of Si(001), a Jahn–Teller-like distortion occurs, leading to a redistribution of the charge and, consequently, to the formation of asymmetric dimers [39].

In section 2, we present the theoretical formalism developed to calculate far-infrared reflectance spectra for the C(001)-(2×1) surface. Besides (section 3), we shall analyze the resonance structure of RAS spectra and compare our results with the predictions of [47–50], where the vibrations of atoms in diamond surfaces have also been studied. Finally, we will compare the FIR-RAS spectra for diamond and silicon surfaces.

2. Theoretical formalism

Let us consider a semi-infinite diamond crystal, occupying the space $z > 0$. An electromagnetic wave, propagating through vacuum ($z < 0$), is incident on the (001)-(2×1) surface of the crystal. The electric field of this wave has the form

$$\mathbf{E}^i = E_0(\cos\phi, \sin\phi, 0)\mathrm{e}^{\mathrm{i}q_z z - \mathrm{i}\omega t}, \tag{1}$$

where ω is the frequency and ϕ is the angle between the vector $\mathbf{E}^i$ and the axis x, which is oriented along the [100] direction. Our goal is to calculate the amplitude of the reflected electromagnetic field. As a first step, we shall analyze the dispersion relations of the vibrational and electromagnetic modes in the bulk of the crystal.

2.1. Dispersion relations of bulk modes

The equations of motion for the atoms in a diamond crystal can be written, within the adiabatic bond charge model (ABCM) [35, 36], as

$$-m\omega^2\mathbf{u}_{is} = \sum_{jt}{}' \Gamma_{isjt}(\mathbf{u}_{jt} - \mathbf{u}_{is}) + \sum_{kn}\Gamma_{iskn}(\mathbf{s}_{kn} - \mathbf{u}_{is}) + qE^{\mathrm{T}}(\mathbf{R}^{\mathrm{ion}}_{is}) \tag{2}$$

$$-m'\omega^2\mathbf{s}_{kn} = \sum_{lm}{}' \Gamma_{knlm}(\mathbf{s}_{lm} - \mathbf{s}_{kn}) + \sum_{jt}\Gamma_{knjt}(\mathbf{u}_{jt} - \mathbf{s}_{kn}) + q'\mathbf{E}^{\mathrm{T}}(\mathbf{R}^{\mathrm{bc}}_{kn}). \tag{3}$$

where $\mathbf{u}_{is}$ is the displacement of the ion of type s ($s = 1, 2$) inside the ith primitive cell of the crystal, with respect to its equilibrium position $\mathbf{R}^{\mathrm{ion}}_{is}$; $\mathbf{s}_{kn}$ is the displacement of the bond charge bc of type n ($n = 1, 2, 3, 4$) with respect to the equilibrium position $\mathbf{R}^{\mathrm{bc}}_{kn}$. m and m' are the masses, $q = 2Ze$ and $q' = -Ze$ (e is the magnitude of the electron charge) are the charges of ions and bond charges, respectively, with the parameter Z to be fitted. An important assumption within the ABCM is that the masses of bond charges are equal to zero ($m' = 0$). The prime in the summation in equation (2) (equation (3)) indicates that $jt \neq is$ [$lm \neq kn$]. The tensors

$$\Gamma_{iskn} = K_{iskn} + \frac{qq'}{\varepsilon_{\mathrm{r}}}P_{iskn} \tag{4}$$

describe the total interaction between the particles is and kn. They contain a mechanical term, K_{iskn}, and a term, associated with the Coulomb interaction, which is proportional to the dipolar tensor

$$P_{iskn} = \nabla_{is}\nabla_{is}\frac{1}{|\mathbf{R}^{\mathrm{ion}}_{is} - \mathbf{R}^{\mathrm{bc}}_{kn}|}. \tag{5}$$

The quantity ε_{r} in equation (4) appears because of the screening of bond charges by the remaining valence electrons.

Assuming that the atomic displacements from their equilibrium positions are small, the terms K_{isjt} and K_{iskn} due to the mechanical interaction are determined by expanding the potential energy of the crystal

$$U^{\mathrm{mech}} = \tfrac{1}{2}\sum_{is,js'}{}'\phi(\mathbf{r}^{\mathrm{ion}}_{is} - \mathbf{r}^{\mathrm{ion}}_{js'}) + \sum_{is,jn}\phi(\mathbf{r}^{\mathrm{ion}}_{is} - \mathbf{r}^{\mathrm{bc}}_{jn}) + \sum_{is}\left(\frac{3}{8(\frac{r_0}{2})^2}\beta\sum_{n,m>n}^{4}[\Delta(\mathbf{r}^{is}_{in}\cdot\mathbf{r}^{is}_{im})]^2\right), \tag{6}$$

near the equilibrium configuration into a Taylor series. The quantity β in (6) is the Keating bond-bending parameter, and r_0 is the equilibrium bond length. Within the harmonic approximation, i.e. retaining up to quadratic terms in such an expansion in particle displacements, the Cartesian components of the mechanical tensors $K^{\mu\nu}_{isjt}$, $K^{\mu\nu}_{iskn}$, $K^{\mu\nu}_{knlm}$ and $K^{\mu\nu}_{knjt}$ acquire the form

$$\begin{aligned} K^{\mu\nu}_{isjt} &= -\phi_{\mu\nu}(\mathbf{R}^{\mathrm{ion}}_{is} - \mathbf{R}^{\mathrm{ion}}_{jt}) \\ K^{\mu\nu}_{iskn} &= -\phi_{\mu\nu}(\mathbf{R}^{\mathrm{ion}}_{is} - \mathbf{R}^{\mathrm{bc}}_{kn}) + \tfrac{3}{4}\beta {\sum_{m=1}^{4}}' \kappa^{\mu}_{iskm}(\kappa^{\nu}_{iskn} + \kappa^{\nu}_{iskm}) \\ K^{\mu\nu}_{knlm} &= \tfrac{3}{4}\beta \kappa^{\mu}_{knlm}\kappa^{\nu}_{knlm} \\ K^{\mu\nu}_{knjt} &= -\phi_{\mu\nu}(\mathbf{R}^{\mathrm{ion}}_{kn} - \mathbf{R}^{\mathrm{bc}}_{jt}) + \tfrac{3}{4}\beta {\sum_{m=1}^{4}}' \kappa^{\mu}_{kmjt}(\kappa^{\nu}_{knjt} + \kappa^{\nu}_{kmjt}) \end{aligned} \tag{7}$$

where

$$\phi_{\mu\nu}(\mathbf{R}^{\mathrm{ion}}_{is} - \mathbf{R}^{\mathrm{ion}}_{jt}) = \left.\frac{\partial^2\phi(r)}{\partial r_\mu \partial r_\nu}\right|_{\mathbf{r}=|\mathbf{R}^{\mathrm{ion}}_{is}-\mathbf{R}^{\mathrm{ion}}_{jt}|} \tag{8}$$

are the components of the second derivatives of the interaction potential between the particles is and jt with respect to their positions of equilibrium, and define the force constants for the interaction between the particles. μ and ν range over the three Cartesian components x, y, z, and the elements κ^{μ}_{iskn} are the components of the unit vector $\hat{\boldsymbol{\kappa}}_{iskn}$ defined along the bond between the particle is and its nearest neighbor kn (its positive direction points to kn).

The last term in equations (2) and (3) describes the interaction of ions and bond charges with the transverse retarded (radiation) field which is produced by the vibration of the charged particles. This field satisfies the wave equation

$$\nabla^2\mathbf{E}^{\mathrm{T}}(\mathbf{r}) + \varepsilon_{\mathrm{r}}\frac{\omega^2}{c^2}\mathbf{E}^{\mathrm{T}}(\mathbf{r}) = -4\pi\frac{\omega^2}{c^2}\mathcal{P}^{\mathrm{T}}\Big[\sum_{jt} q\mathbf{u}_{jt}\delta(\mathbf{r} - \mathbf{R}^{\mathrm{ion}}_{jt}) + \sum_{jn} q'\mathbf{s}_{jn}\delta(\mathbf{r} - \mathbf{R}^{\mathrm{bc}}_{jn})\Big], \tag{9}$$

where

$$\mathcal{P}^{\mathrm{T}}(\mathbf{k}) = \mathbf{I} - (\mathbf{kk}/k^2) \tag{10}$$

is the transverse projection operator ($\mathbf{I}$ is the identity matrix), $\delta(\mathbf{r})$ is the Dirac delta function and c is the light velocity in vacuum.

The solutions for equations (2), (3) and (9) in the crystal bulk have the form of Bloch waves:

$$\mathbf{u}_{is} = \mathbf{u}_s(\mathbf{k})\mathrm{e}^{\mathrm{i}\mathbf{k}\cdot\mathbf{R}^{\mathrm{ion}}_{is}}, \tag{11}$$

$$\mathbf{s}_{kn} = \mathbf{s}_n(\mathbf{k})\mathrm{e}^{\mathrm{i}\mathbf{k}\cdot\mathbf{R}^{\mathrm{bc}}_{kn}}, \tag{12}$$

$$\mathbf{E}^{\mathrm{T}}(\mathbf{r}) = \sum_{\mathbf{K}} \mathbf{E}^{\mathrm{T}}(\mathbf{k},\mathbf{K})\mathrm{e}^{\mathrm{i}(\mathbf{k}+\mathbf{K})\cdot\mathbf{r}}. \tag{13}$$

In principle, the sum in (13) ranges over all the vectors $\mathbf{K}$ of the reciprocal lattice. However, the main contribution to the radiation field $\mathbf{E}^{\mathrm{T}}(\mathbf{r})$ is attributed to the first term of the sum ($\mathbf{K} = \mathbf{0}$), which represents the macroscopic electric field. Indeed, after substituting equation (13) into equation (9), we obtain explicit expressions for the coefficients $\mathbf{E}^{\mathrm{T}}(\mathbf{k},\mathbf{K})$, according to which the terms with $\mathbf{K} \neq \mathbf{0}$ in the expansion (13) are of the order of $(\omega a/c)^2 \ll 1$ (a is the lattice constant), whereas the coefficient $\mathbf{E}^{\mathrm{T}}(\mathbf{k},\mathbf{0}) \approx (\omega/ck)$ is of the order of one. Neglecting the microscopic fluctuations in the transverse field $\mathbf{E}^{\mathrm{T}}(\mathbf{r})$ [18, 30, 32], we get

$$\mathbf{E}^{\mathrm{T}}(\mathbf{r}) \approx \mathbf{E}^{\mathrm{T}}(\mathbf{k},\mathbf{0})\mathrm{e}^{\mathrm{i}\mathbf{k}\cdot\mathbf{r}}, \tag{14}$$

where

$$\mathbf{E}^{\mathrm{T}}(\mathbf{k},\mathbf{0}) = \frac{1}{\Omega c^2}\left(\frac{4\pi\omega^2}{k^2 - (\omega^2/c^2)\varepsilon_{\mathrm{r}}}\right) \times \mathcal{P}^{\mathrm{T}}\Big[\sum_{t=1}^{2} q\mathbf{u}_t(\mathbf{k}) + \sum_{n=1}^{4} q'\mathbf{s}_n(\mathbf{k})\Big], \tag{15}$$

and Ω is the volume of the primitive cell. Because of the normal incidence of light (see equation (1)), the Bloch wavevector $\mathbf{k}$ in equations (11), (12), and (14) is chosen to be parallel to the [0 0 1] direction, i.e. $\mathbf{k} = (0, 0, k_z)$.

We can eliminate the amplitudes $\mathbf{s}_n(k_z)$ and $\mathbf{E}^{\mathrm{T}}(\mathbf{k},\mathbf{0})$ from the system of equations (2), (3) and (9) and obtain a system of equations exclusively for the amplitudes of the ion displacements $\mathbf{u}_s(k_z)$ ($s = 1, 2$):

$$-m\omega^2\mathbf{u}_1 = U_{11}\mathbf{u}_1 + U_{12}\mathbf{u}_2 \qquad -m\omega^2\mathbf{u}_2 = U_{21}\mathbf{u}_2 + U_{22}\mathbf{u}_2. \tag{16}$$

For the diamond crystal structure the matrices U_{st} ($s, t = 1, 2$) have the form

$$U_{11} = U_{22} = \begin{pmatrix} U^{xx}_{11} & 0 & 0 \\ 0 & U^{yy}_{11} & 0 \\ 0 & 0 & U^{zz}_{11} \end{pmatrix}, \tag{17}$$

$$U_{12} = U^*_{21} = \begin{pmatrix} U^{xx}_{12} & U^{xy}_{12} & 0 \\ U^{yx}_{12} & U^{yy}_{12} & 0 \\ 0 & 0 & U^{zz}_{12} \end{pmatrix}, \tag{18}$$

with $U^{xx}_{11} = U^{yy}_{11}$, $U^{xx}_{12} = U^{yy}_{12}$, $U^{xy}_{12} = U^{yx}_{12}$. We do not present the explicit expressions for the elements of the matrices U_{11} and U_{12} here because of their cumbersome form.

We, further, eliminate the amplitude $\mathbf{u}_2$ from equations (16). Using (17) and (18), we find

$$M\mathbf{u}_1 = 0, \qquad M = [(m\omega^2 I + U_{11})^2 - U_{12}U^*_{12}]. \tag{19}$$

The matrix M is diagonal since the product $U_{12}U^*_{12}$ turns out to be diagonal. Hence, the calculation of the dispersion relations for the bulk phonon modes is straightforwardly carried out.

The transverse phononic modes are degenerated ($M^{xx} = M^{yy}$) and their dispersion relation is given by

$$m^2\omega^4 + 2m\omega^2 U^{xx}_{11} + (U^{xx}_{11})^2 - (U^{xx}_{12})^2 - |U^{xy}_{12}|^2 = 0. \tag{20}$$

On the other hand the dispersion relation of longitudinal phonon modes can be written as

$$m^2\omega^4 + 2m\omega^2 U^{zz}_{11} + (U^{zz}_{11})^2 - (U^{zz}_{12})^2 = 0. \tag{21}$$

In figure 1 we present the bulk phononic dispersion curves ($\omega = \omega(k_z)$) for C. The ABCM parameters used are shown in table 1, being different from those proposed by Weber [36]. Other diamond parameters are: the ions mass $m = 12.011u$

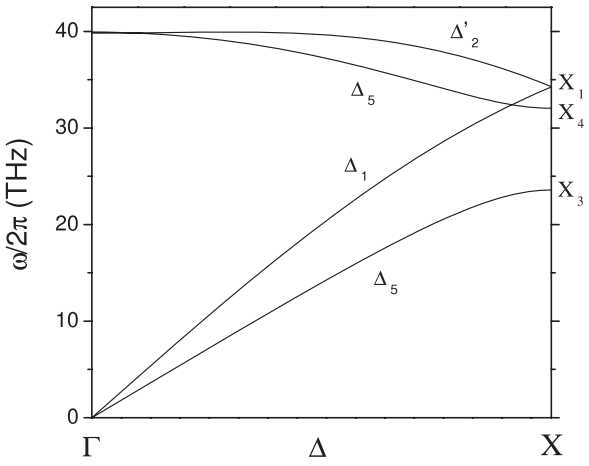

Figure 1. Dispersion relation of bulk phonons for C in the [001] direction, calculated with the ABCM.

Table 1. ABCM parameters used in calculating the phonon dispersion relations. All the force constants are given in units of e^2/V_c, V_c is the volume of the primitive cell in the bulk (b) and r_0 is the equilibrium bond length between the nearest neighboring ions.

$\phi''_{i-i}(b)$	$\phi''_{i-\mathrm{bc}}(b)$	$\phi'_{i-i}(b)/r_0$	$\phi'_{i-\mathrm{bc}}(b)/r_0$	$\beta(b)$	$Z^2(b)/\epsilon_\mathrm{r}$
14.63	−4.27	46.13	−44.07	8.72	0.177

and the lattice constant $a = 3.57$ Å. The phononic bands for C, obtained with the ABCM, agree with the experimental phononic bands [51] (see also table 2). Notice that our results reproduce the maximum of the optical phonon branch which occurs along the [001] direction. It should also be emphasized that, unlike Weber numerical calculations [35, 36], we have incorporated the radiation field (14) in the equations of motion (2) and (3). The contribution of this field to the dispersion of phonons with $k_z \sim 1/a$ is negligible as $(\omega a/c)^2 \ll 1$.

The dependence of the components of the matrices U_{st} $(s, t = 1, 2)$ in equation (19) upon the radiated transverse field is manifested at small values of the wavenumber as $k_z \sim \omega/c \ll 1/a$. We have derived the dispersion relation of photon-like modes by eliminating the displacements $\mathbf{s}_n(k_z)$ and $\mathbf{u}_s(k_z)$ from the system of equations (2), (3) and (9) in the limiting case $k_z a \to 0$. The resulting dispersion relation can be written as

$$k_z^E = \frac{\omega}{c}\sqrt{\epsilon_\mathrm{r} + \Delta\epsilon_\mathrm{bc}}. \qquad (22)$$

As was expected, it corresponds to the dispersion relation of an electromagnetic wave propagating in a medium with dielectric constant $\epsilon = \epsilon_\mathrm{r} + \Delta\epsilon_\mathrm{bc}$, where $\Delta\epsilon_\mathrm{bc}$ is the contribution to the dielectric function of the medium due to the bond charges. Using the value $\epsilon = 5.7$ for diamond, we found $Z = 1.06$, $\epsilon_\mathrm{r} = 6.35$ and $\Delta\epsilon_\mathrm{bc} = -0.65$.

Above, we have calculated the dispersion relations $\omega = \omega(k_z)$ for the normal bulk modes. However, in the investigation of the excitation of vibrational modes of surface atoms with light, we need to solve the inverse problem, that is, given a frequency ω it is necessary to find all the wavenumbers k_z, being either real or complex and satisfying the dispersion

Table 2. Experimental values [51] for the frequencies ν $(=\omega/2\pi)$ of bulk phonons at X and Γ points (in THz units) for C and its comparison with the frequency values predicted by the ABCM with the parameters of table 1.

	Experiment	ABCM
$\nu_{\mathrm{LTO}}(\Gamma)$	39.9	39.9
$\nu_{\mathrm{LAO}}(\mathrm{X}_1)$	35.5	34.3
$\nu_{\mathrm{TO}}(\mathrm{X}_4)$	32.0	32.0
$\nu_{\mathrm{TA}}(\mathrm{X}_3)$	24.2	23.6

relations (20)–(22). The problem is not trivial since there are an infinite number of solutions. A set of solutions corresponds to the transverse and longitudinal phononic modes obtained from equations (20) and (21). Another set of solutions is found from the expression (22) for the photonic modes with small k_z (k_z^E). The real values of k_z correspond to waves propagating through the lattice, whereas the values of k_z with an imaginary part are associated with evanescent waves, which can be excited at the surface of a semi-infinite crystal. To simplify the problem, i.e. to obtain a finite number of solutions, $k_z(\omega)$, we have neglected the Coulomb interaction between (001) planes of charged particles that are separated by a distance larger than, or equal to, the constant lattice a. This approximation is good enough since such an interaction decays exponentially [32]. As a result, the approximation leads to sixth-degree polynomial equations $P_6(x) = 0$, with $x = \cos(k_z a/2)$, for both transverse (T) and longitudinal (L) phonon modes. The proper phononic ($k_z^{\mathrm{T}}(\omega)$, $k_z^{\mathrm{L}}(\omega)$) and photonic $k_z^E(\omega)$ solutions are chosen by introducing a small damping γ_0 ($\omega \to \omega + \mathrm{i}\gamma_0$) and taking the roots with a positive imaginary part ($\mathrm{Im}\, k_z > 0$), since such modes decay towards the crystal bulk.

2.2. *Expansion in bulk modes*

As already mentioned, the illuminated C(001) surface is assumed to have a 2×1 reconstruction pattern with symmetric dimers (see figures 2 and 3). In accordance with the ABCM for a semi-infinite crystal [47], bond charges, $-Ze$, are placed midway between neighboring C ions of charge $2Ze$. The crystal surface is formed by the ions $si_1, si_2, \ldots, si_6$ and the bond charges $sc_1, sc_2, \ldots, sc_{12}$. The dimer ions si_1 and si_2 are assumed to be at $z = a/8$. The positions of the surface dangling bond charges (sc_1, sc_2, and sc_3) were determined by the maxima in the valence-electron density, which was calculated in [47] by using the density-functional theory. The charge $-Ze$ is distributed between the dangling charges so that each one is equal to $-Ze/3$ ($q'_1 = q'_2 = q'_3 = -Ze/3$).

The equations of motion for the charged particles with bulk-like equilibrium positions in the semi-infinite crystal can be written as in equations (2) and (3), but with summations ranging only over occupied sites. Such a system is complemented by the equations of motion for the surface charged particles (the ions $si_1, si_2, \ldots, si_6$ and the bond charges $sc_1, sc_2, \ldots, sc_{12}$). Here, it should be mentioned that the potential energy (6) is expressed in terms of the scalar products of the bond radius between ions and charges, both in the bulk and on the surface. In addition, since the scalar

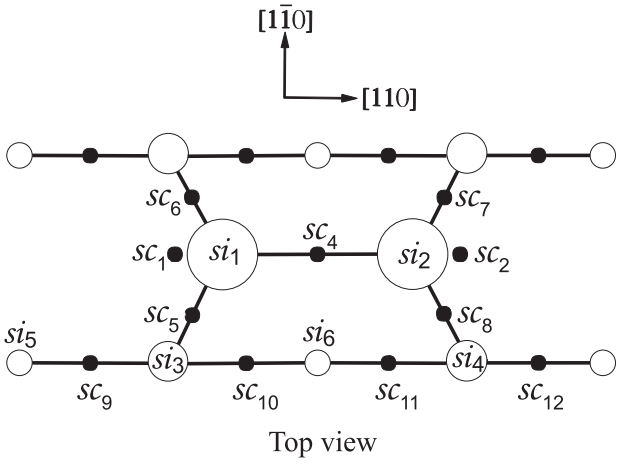

Figure 2. Schematic top view of the C(001)-(2 × 1) surface. The surface ions and bond charges are labeled si_l and sc_p ($l = 1, 2, \ldots, 6$; $p = 1, 2, \ldots, 12$), respectively.

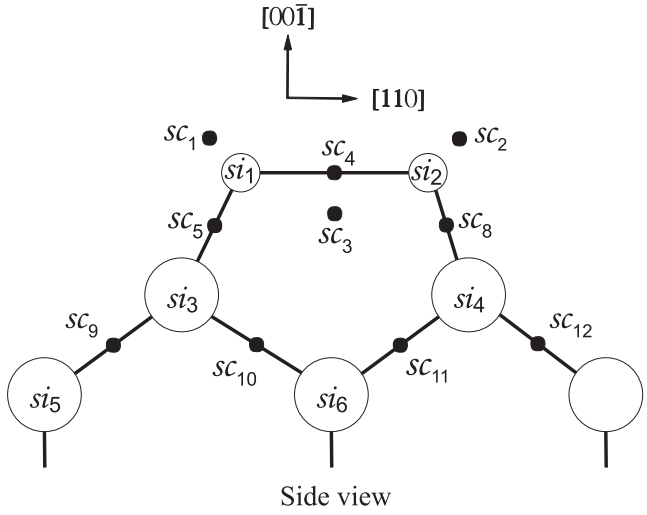

Figure 3. Schematic side view of the C(001)-(2 × 1) surface.

products do not change under rotations, the energy of the truncated crystal is not altered under a rotation.

For normal-incidence geometry, the displacements of the ions and bond charges on the reconstructed surface, and the electric field (in $z > 0$) can be expressed as

$$\mathbf{u}_\ell^{\mathrm{si}} = \sum_{\mathbf{Q}} \mathbf{u}(\mathbf{Q}, z_\ell) \mathrm{e}^{\mathrm{i}\mathbf{Q}\cdot\mathbf{R}^{\mathrm{si}}_{||,\ell}}, \qquad \ell = 1, \ldots, 6, \tag{23}$$

$$\mathbf{s}_p^{\mathrm{sc}} = \sum_{\mathbf{Q}} \mathbf{s}(\mathbf{Q}, z_p) \mathrm{e}^{\mathrm{i}\mathbf{Q}\cdot\mathbf{R}^{\mathrm{sc}}_{||,p}}, \qquad p = 1, \ldots, 12, \tag{24}$$

$$\mathbf{E}^{\mathrm{T}}(\mathbf{r}) = \sum_{\mathbf{Q}} \mathbf{E}^{\mathrm{T}}(\mathbf{Q}, z) \mathrm{e}^{\mathrm{i}\mathbf{Q}\cdot\mathbf{r}_{||}}. \tag{25}$$

Here, the vector $\mathbf{r}_{||}$ is the projection of the position vector $\mathbf{r}$ on the xy-plane ($\mathbf{r}_{||} = (x, y, 0)$), and the summations range over the reciprocal vectors of the reconstructed surface of the crystal. As follows from the wave equation (9), the terms with $\mathbf{Q} \neq \mathbf{0}$ in the expression (25) for the electric field, which are associated with the phenomenon of light diffraction, can be neglected, since their relative contribution turns out to be quadratic in the parameter $(\omega a/c)^2 \ll 1$. Therefore, $\mathbf{E}^{\mathrm{T}}(\mathbf{r}) \approx \mathbf{E}^{\mathrm{T}}(\mathbf{Q} = 0, z) \equiv \mathbf{E}^{\mathrm{T}}(z)$. Below, we also neglect the terms with $\mathbf{Q} \neq 0$ in the expansion for the displacements of both surface ($\mathbf{u}_\ell^{\mathrm{si}}$ (23), $\mathbf{s}_p^{\mathrm{sc}}$ (24)) and bulk particles ($\mathbf{u}_{it}$, $\mathbf{s}_{jn}$). The latter are expanded into bulk normal modes [52, 53]:

$$\mathbf{u}_{it} = \sum_l \sum_{k_z^l} \mathbf{u}_t(k_z^l, l) \mathrm{e}^{\mathrm{i}k_z^l z_{it}} \tag{26}$$

$$\mathbf{s}_{jn} = \sum_l \sum_{k_z^l} \mathbf{s}_n(k_z^l, l) \mathrm{e}^{\mathrm{i}k_z^l z_{jn}}, \tag{27}$$

where $\mathbf{u}_t(k_z^l, l)$ and $\mathbf{s}_n(k_z^l, l)$ are the polarization vectors of the bulk (both phonon and photon) modes, corresponding to the solutions k_z^l for the dispersion relations (equations (20)–(22)). The super-index l denotes the branches: $l = T_1, T_2$ label the two *transverse phonon* polarizations, $l = L$ indicates the *longitudinal phonon* polarization and $l = E_1, E_2$ correspond to the two *transverse* polarizations of the *photon* modes. The vectors $\mathbf{u}_t(k_z^l, l)$ and $\mathbf{s}_n(k_z^l, l)$ are found by imposing that the displacements $\mathbf{u}_{it}$ and $\mathbf{s}_{jn}$ in (26) and (27) satisfy the equations of motion for the charges of the semi-infinite crystal. The system of equations becomes finite thanks to the truncation of the Coulomb interaction carried out above. Thus, the resulting finite system is given by the equations of motion for the 18 surface particles shown in figures 2 and 3 (i.e. $si_1, si_2, \ldots, si_6$ and $sc_1, sc_2, \ldots, sc_{12}$), and 6 particles of the first (closer to the crystal surface) bulk-like primitive cell, whose displacements are coupled to the displacements of the surface particles. The system is closed with the expansion for the macroscopic electric field $\mathbf{E}^{\mathrm{T}}(z)$ inside the semi-infinite crystal into bulk modes:

$$\mathbf{E}^{\mathrm{T}}(z) = \sum_l \sum_{k_z^l} \mathbf{E}^{\mathrm{T}}(k_z^l, l) \mathrm{e}^{\mathrm{i}k_z^l z}, \tag{28}$$

where $\mathbf{E}^{\mathrm{T}}(k_z^l, l)$ is expressed in terms of the amplitudes $\mathbf{u}_t(k_z^l, l)$ and $\mathbf{s}_n(k_z^l, l)$ as (equation (15)):

$$\mathbf{E}^{\mathrm{T}}(k_z^l, l) = \frac{1}{\Omega c^2} \left(\frac{4\pi\omega^2}{(k_z^l)^2 - (\omega^2/c^2)\varepsilon_{\mathrm{r}}} \right) \times \mathcal{P}^{\mathrm{T}}(k_z^l) \Big[\sum_{t=1}^{2} q \mathbf{u}_t(k_z^l, l) + \sum_{n}^{4} q' \mathbf{s}_n(k_z^l, l) \Big]. \tag{29}$$

We should emphasize that the expansion (28) for the macroscopic electric field $\mathbf{E}^{\mathrm{T}}(z)$ contains only transverse bulk modes ($l = T_1, T_2, E_1, E_2$).

2.3. Calculation of reflectivity

As was mentioned above, the components $\mathbf{E}^{\mathrm{T}}(\mathbf{Q}, z)$ (with $\mathbf{Q} \neq 0$) of the electric field $\mathbf{E}^{\mathrm{T}}$ (25) are negligible ($\mathbf{E}^{\mathrm{T}}(\mathbf{r}) \approx \mathbf{E}^{\mathrm{T}}(\mathbf{Q} = 0, z)$). Therefore, the light must be reflected specularly from the crystal surface and the electric field of the reflected wave can be written in the form

$$\mathbf{E}^{\mathrm{r}} = (E_x^{\mathrm{r}}, E_y^{\mathrm{r}}, 0) \mathrm{e}^{-\mathrm{i}q_z - \mathrm{i}\omega t}. \tag{30}$$

In order to calculate the amplitudes E_x^{r} and E_y^{r} of the reflected electromagnetic wave (30), we should apply Maxwell

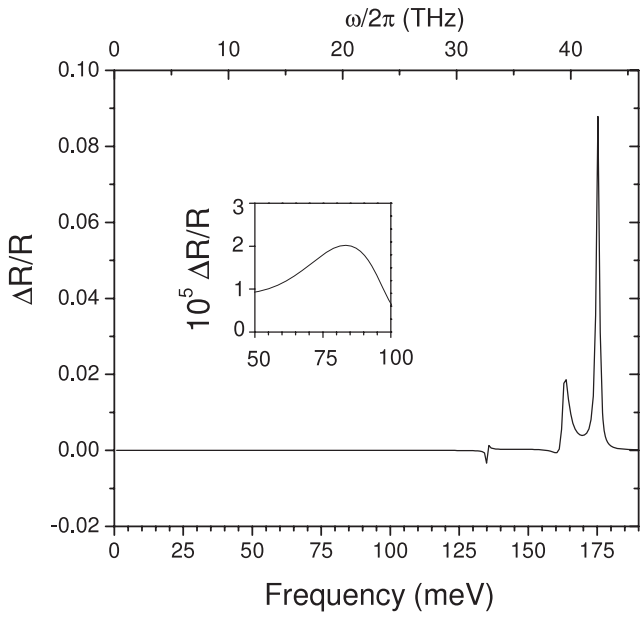

Figure 4. Deviation of the reflectivity with respect to the Fresnel formula for the C(001)-(2 × 1) surface and incident light with a polarization vector along the [1 $\bar{1}$ 0] direction.

boundary conditions, i.e. the continuity of the tangential components of the electric and magnetic fields at the vacuum–diamond interface ($z = 0$). Afterwards, a relation for the components of transverse field $\mathbf{E}^{\mathrm{T}}(z)$, and its normal derivative $\mathrm{d}\mathbf{E}^{\mathrm{T}}(z)/\mathrm{d}z$ at $z = 0$, with the amplitudes of the incident (equation (1)) and reflected (equation (30)) fields is derived:

$$E_x^{\mathrm{T}}(0) = E_0\cos\phi + E_x^{\mathrm{r}}, \qquad E_y^{\mathrm{T}}(0) = E_0\sin\phi + E_y^{\mathrm{r}}, \quad (31)$$

$$\frac{\mathrm{d}E_x^{\mathrm{T}}(0)}{\mathrm{d}z} = \mathrm{i}q_z(E_0\cos\phi - E_x^{\mathrm{r}}),$$
$$\frac{\mathrm{d}E_y^{\mathrm{T}}(0)}{\mathrm{d}z} = \mathrm{i}q_z(E_0\sin\phi - E_y^{\mathrm{r}}). \quad (32)$$

The values of $E_x^{\mathrm{T}}(0)$ and $E_y^{\mathrm{T}}(0)$ in (31) are coupled to bulk displacements according to equations (28) and (29). The resulting system of equations for the amplitudes has to be closed with an accurate relation between $\mathbf{E}^{\mathrm{T}}(0)$ and $\mathrm{d}\mathbf{E}^{\mathrm{T}}(0)/\mathrm{d}z$. In order to obtain it, we have solved the wave equation (9) for the irradiated transverse field inside the semi-infinite medium ($z > 0$) by applying the standard Fourier transform method. After using the expansions (26) and (27) for the ion and charge displacements into bulk modes, we get

$$\mathbf{E}^{\mathrm{T}}(0) = -\frac{\mathrm{i}}{k_{\mathrm{r}}}\frac{\mathrm{d}\mathbf{E}^{\mathrm{T}}}{\mathrm{d}z}\bigg|_{z=0} + \frac{4\pi\mathrm{i}\omega^2}{k_{\mathrm{r}}a^2c^2}\mathcal{P}^{\mathrm{T}}\Bigg(\sum_{\ell=1}^{6} q\mathbf{u}_\ell^{\mathrm{si}}(k_z)\exp(\mathrm{i}k_{\mathrm{r}}z_\ell)$$
$$+ \sum_{p=1}^{12} q'_p\mathbf{s}_p^{\mathrm{sc}}(k_z)\exp(\mathrm{i}k_{\mathrm{r}}z_p)$$
$$+ \sum_{t=1}^{2}\sum_{l}\sum_{k_z^l} q\mathbf{u}_t(k_z^l)\left[\frac{\exp(\mathrm{i}(k_z^l + k_{\mathrm{r}})z_t^{(1)})}{1-\exp(\mathrm{i}(k_z^l + k_{\mathrm{r}})a/2)}\right]$$
$$+ \sum_{n=1}^{4}\sum_{l}\sum_{k_z^l} q'\mathbf{s}_n(k_z^l)\left[\frac{\exp(\mathrm{i}(k_z^l + k_{\mathrm{r}})z_n^{(1)})}{1-\exp(\mathrm{i}(k_z^l + k_{\mathrm{r}})a/2)}\right]\Bigg), \quad (33)$$

Table 3. Values for the force constants on the surface C(001)-(2 × 1) (s) in units of e^2/V_c, used in calculating the reflectivity.

$\phi''_{i-i}(s)$	$\phi''_{i-\mathrm{bc}}(s)$	$\phi'_{i-i}(s)/r_0$	$\phi'_{i-\mathrm{bc}}(s)/r_0$	$\beta(s)$	$Z^2(s)/\epsilon_{\mathrm{r}}$
14.63	−4.27	46.13	−2.5	8.72	0.177

where $k_{\mathrm{r}} = \sqrt{\epsilon_{\mathrm{r}}}\omega/c$. The quantities $z_t^{(1)}$ ($t = 1, 2$) and $z_n^{(1)}$ ($n = 1, \ldots, 4$) in equation (33) indicate the positions of ions and bound charges of the first bulk-like primitive cell below the layer of surfaces ions (si) and bond charges (sc), respectively (see figures 2 and 3).

After solving the resulting system of algebraic equations for the components of the displacements vectors $\mathbf{u}_t(k_z^l)$, $\mathbf{s}_n(k_z^l)$, $\mathbf{u}_\ell^{\mathrm{si}}$, $\mathbf{s}_p^{\mathrm{sc}}$, the electric field $\mathbf{E}^{\mathrm{T}}$ and its derivative $\mathrm{d}\mathbf{E}^{\mathrm{T}}/\mathrm{d}z$ at $z = 0$, and the components of the reflected electromagnetic wave $(E_x^{\mathrm{r}}, E_y^{\mathrm{r}})$, the normal-incidence reflectivity is straightforwardly calculated with the formula:

$$R = \left|\frac{E_x^{\mathrm{r}}}{E_0}\right|^2 + \left|\frac{E_y^{\mathrm{r}}}{E_0}\right|^2. \quad (34)$$

Below, we shall present results for the reflectance difference spectrum given by the expression

$$\frac{\Delta R}{R} = \frac{R - R_{\mathrm{F}}}{R}, \quad (35)$$

which determines the deviation of the reflectivity R with respect to the reflectivity R_{F}, calculated by using the Fresnel formula for a medium with dielectric constant $\epsilon = \epsilon_{\mathrm{r}} + \Delta\epsilon_{\mathrm{bc}}$:

$$R_{\mathrm{F}} = \left|\frac{1-\sqrt{\epsilon}}{1+\sqrt{\epsilon}}\right|. \quad (36)$$

3. Reflectance anisotropy spectra

The deviations of the normal-incidence reflectivity from the Fresnel formula $\Delta R/R$ for the C(001)-(2 × 1) surface are presented in figures 4 and 5 for two different polarizations of the incident electric field: parallel (p) (figure 4) and perpendicular (s) (figure 5) to the direction of dimer rows (i.e. with respect to the [1$\bar{1}$0] direction). We also present the FIR reflectance anisotropy spectrum (figure 6), obtained by subtracting the spectrum for p polarization (figure 4) from the spectrum for s polarization (figure 5). Precisely, such a spectrum (figure 6) could be experimentally measured. In calculating the spectra, the data used for the relaxed geometry of the C(001)-(2 × 1) surface were taken from [47], where the computations are based on the local density approximation (LDA) of the density-functional theory. So, the surface has symmetric dimers (figures 2 and 3) with a bond length of 1.38 Å, which agrees with previously reported results (see, for example, [38–42, 49, 50]). As was mentioned in section 4, the orbital lobes are represented by three bond charges ($q'_1 = q'_2 = q'_3 = -Ze/3$) at points corresponding to the maxima of the electronic charge density. The values of the force constants on the surface, used here, are shown in table 3.

The reflectance difference spectra (figures 4 and 5) exhibit resonances at $\hbar\omega = 83$, 134.9, 162.9, and 175.2 meV, with

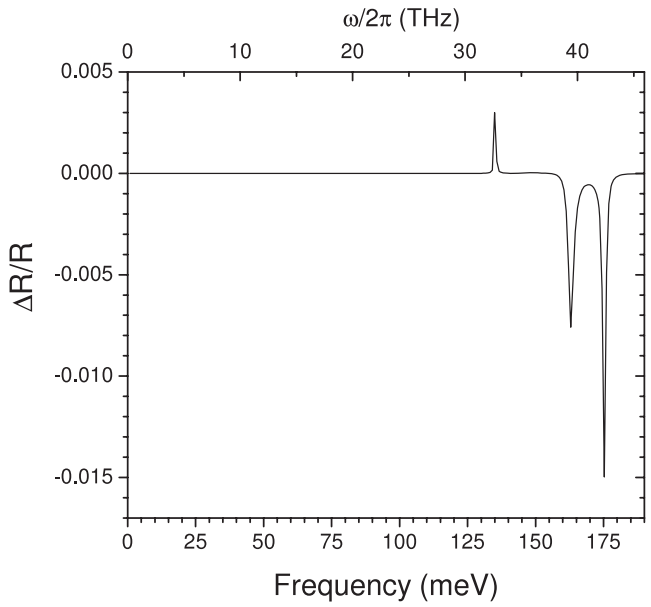

Figure 5. Deviation of the reflectivity with respect to the Fresnel formula for the C(001)-(2 × 1) surface and incident light with a polarization vector along the [1 1 0] direction.

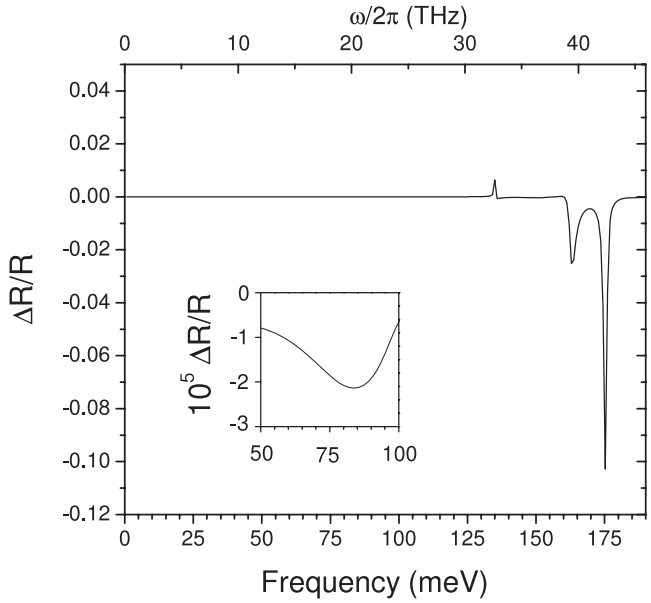

Figure 6. Reflectance anisotropy spectrum obtained by subtracting the spectrum in figure 4 from that in figure 5.

relative intensities of the order of 10^{-5}–10^{-2}, which depend on the polarization of the incident light. All these resonances should be associated with surface phonons at the $\bar{\Gamma}$ point, since in the calculations we have expanded the displacements of the ions and charges in the semi-infinite crystal into bulk normal modes with zero parallel wavevector, only (see section 2.2). Note that the deviations from the Fresnel formula turn out to be more prominent for light with a polarization parallel to the dimer rows (compare figures 4 and 5). The RAS resonances (figure 6) appear in the frequency regions of the 700 cm^{-1} (87 meV), 1015 cm^{-1} (126 meV) and the 1225 cm^{-1}

Table 4. Frequencies (in meV) of electromagnetically excited surface phonons at $\bar{\Gamma}$ for the C(001)-(2 × 1) surface, corresponding to the resonances in the reflectance anisotropy spectra (figure 6). The symmetries (even or odd) of phonon modes with respect to the mirror plane perpendicular to the dimer rows are also indicated.

RAS	ABCM[a]	*Ab initio*[b]	HREELS[c]
83	90/even	89/even (∼87.5/even)	87(92)
134.9	133/even	140/even (∼126.3/odd)	126(135)
162.9	169/even	∼164/odd (∼162.8/odd)	∼152(164)
175.2	176/even	174/even (184.6/even)	∼152(172)

[a] Reference [47]. [b] References [47] ([49]).
[c] References [54, 55] ([48]).

(152 meV) bands, observed by means of HREELS in [54, 55] (correspondingly, figures 1 and 7 therein). The HREELS peak at the highest frequency (152 meV) is wide and is composed of various phonon resonances. Also, RAS features are very close to the well-defined features at $\hbar\omega$ =92, 135, 164, and 172 meV in the EELS spectrum reported in [48] (figure 2 therein). The frequencies and symmetries of the corresponding surface phonons at the $\bar{\Gamma}$ point, predicted in [47–50] by employing *ab initio* techniques and an adiabatic bond charge model, are indicated in table 4.

The two highest RAS resonances at 162.9 and 175.2 meV (figure 6) for the C(001)-(2 × 1) surface correspond to the two localized phonon modes, at 169 and 176 meV, which are above the bulk continuum in the phonon dispersion calculated with the ABCM in [47]. These localized modes give rise to two high-frequency peaks in the density of states (DOS) on the C(001)-(2 × 1) surface (peaks labeled S^4 in figure 9 of [47]). The RAS feature at the highest frequency, 175.2 meV, corresponds to a dimer stretch mode [47, 49] of even symmetry, which results from the opposing vibrations of the dimer ions (si_1 and si_2) on the mirror plane perpendicular to the dimer row direction. The resonance at 162.9 meV, appearing slightly below the frequency of the bulk optical phonon (164 meV), is associated with the even mode at 169 meV predicted in [47]. The small difference of 6 meV in the energy localization for such a phonon mode is due to the use of different ABCM fitting parameters. In our calculations, we have chosen the ABCM parameters among various solution sets so that both bulk phonon dispersion curves (figure 1) are well reproduced and the RAS features agree with the resonances observed in the EELS experiment [48] (see table 4). Finally, the RAS features at 83 and 134.9 meV compare well with the zone-center surface phonon frequencies from *ab initio* and ABCM calculations, indicated in our table 4 (see also table III in [47]). It should be mentioned that the even surface phonon modes (vibrations on the mirror plane) can be excited by light with a polarization vector parallel to the dimer rows (see figure 4) thanks to the coupling of the components of the particle displacements at the reconstructed surface.

We should note that features, associated with localized modes just above the bulk continuum in the phonon dispersion, were also predicted for the Si(001)-(2 × 1) surface in the asymmetric dimer geometry, at 66.84 (67.1) meV and 68.06 (69.25) meV in [34] ([37]). In addition, the low-frequency resonances at 47.92 and 57.26 meV in the RAS spectrum

for the Si(001)-(2 × 1) surface [34] are relatively strong, unlike low-frequencies resonances at 83 and 134.9 meV for the C surface (compare figure 2 of [34] with our figure 6). The resonance structure in reflectance anisotropy spectra for the Si surface also turns out to be similar to that observed in RAS spectra for the Ge(001)-(2 × 1) surface with tilted dimers [56]. Therefore, the difference in the resonance structure of reflectance anisotropy spectra for the C(001)-(2 × 1) surface, compared with the corresponding Ge and Si surfaces, can be attributed to the symmetric dimer geometry of the diamond surface. Significantly, the difference of RAS spectra for C(001) and Si(001) surfaces is observed not only in the far infrared, but also in the visible and ultraviolet frequency ranges [45, 46] as it was commented upon in section 1. Nevertheless, experiments with FIR-RAS are needed to elucidate the differences of the phonon–photon coupling at (001) surfaces of diamond-type crystals.

4. Conclusion

We have developed a theoretical formalism for calculating far-infrared reflectance anisotropy spectra (FIR-RAS) within the empirical adiabatic bond charge model. The formalism has been applied to study the photon–phonon coupling at C(001)-(2 × 1) surfaces with a symmetric dimer geometry. The spectra of FIR-RAS calculated here show a resonance structure due to the electromagnetic excitation of zone-center phonons at frequencies that correspond to frequency bands previously measured with HREELS [48, 54, 55], and predicted with the ABCM [47, 48] and first principle calculations [48–50]. It was found that the highest-frequency surface phonon modes, lying just above the bulk continuum in the phonon dispersion, yield huge resonances, of the order of 10^{-2}, in the reflectance anisotropy spectra. In comparison with silicon and germanium (001)-(2 × 1) surfaces, characterized by an asymmetric dimer reconstruction, the spectrum of FIR-RAS for the C(001)-(2 × 1) surface, with a symmetric dimer, is noticeably different because of the weak manifestation of low-frequency zone-center surface phonons in the diamond case.

Acknowledgment

This work was partially supported by CONACYT under grant SEP-2004-C01-46425.

References

[1] Ibach H and Mills D L 1984 *Electron Energy Loss Spectroscopy of Surface Vibrations* (New York: Academic) chapter 3
[2] Wallis R F 1994 *Surf. Sci.* **299/300** 612
[3] Benedek G and Toennies J P 1994 *Surf. Sci.* **299/300** 587
[4] Srivastava G P 1997 *Rep. Prog. Phys.* **60** 561
[5] Srivastava G P 1999 *Theoretical Modelling of Semiconductor Surfaces* (Singapore: World Scientific) chapter 8
[6] Fritsch J and Schröder U 1999 *Phys. Rep.* **309** 209
[7] Nienhaus H and Monch W 1994 *Phys. Rev.* B **50** 11750
[8] Nienhaus H and Monch W 1995 *Surf. Sci.* **328** L561
[9] Jakob P 1996 *Phys. Rev. Lett.* **77** 4229
[10] Jianfeng X and Youwei D 1996 *Phys. Lett.* A **215** 215
[11] Hinrichs K, Gensch M, Röseler A and Esser N 2004 *J. Phys.: Condens. Matter* **16** S4335
[12] Marschall N and Fischer B 1972 *Phys. Rev. Lett.* **28** 811
[13] Barker A S 1972 *Phys. Rev. Lett.* **28** 892
[14] Chen Y J, Burstein E and Mills D L 1975 *Phys. Rev. Lett.* **34** 1516
[15] Nkoma J S and Loudon R 1975 *J. Phys. C: Solid State Phys.* **8** 1950
[16] Peremans A and Tadjeddine A 1994 *Phys. Rev. Lett.* **73** 3010
[17] Tadjeddine A, Peremans A and Guyot-Sionnest P 1995 *Surf. Sci.* **335** 210
[18] Mochán W L and Récamier J 1989 *Phys. Rev. Lett.* **63** 2100
[19] Aspnes D E and Studna A A 1985 *Phys. Rev. Lett.* **54** 1956
[20] Koch M S, Acher O, Omnes F, Defour M, Drévillon B and Razeghi M 1991 *J. Appl. Phys.* **69** 1389
[21] Kamiya I, Aspnes D E, Tanaka H, Florez L T, Harbison J P and Bhat R 1992 *Phys. Rev. Lett.* **68** 627
[22] Kolb D M, Boeck W, Ho K-M and Liu S H 1981 *Phys. Rev. Lett.* **47** 1921
[23] Aspnes D E, Colas E, Studna A A, Bhat R, Koza M A and Keramidas V G 1988 *Phys. Rev. Lett.* **61** 2782
[24] Noguez C and Ulloa S E 1996 *Phys. Rev.* B **53** 13138
[25] Hahn P H, Schmidt W G and Bechstedt F 2002 *Phys. Rev. Lett.* **88** 016402
[26] Vázquez-Nava R A, Mendoza B S and Castillo C 2004 *Phys. Rev.* B **70** 165306
[27] Vázquez-Nava R A, Mendoza B S and Arzate N 2005 *Phys. Status Solidi* b **442** 3022
[28] Lastras-Martínez L F, Flores-Camacho J M, Lastras-Martínez A, Balderas-Navarro R E and Cardona M 2006 *Phys. Rev. Lett.* **96** 047402
[29] Lastras-Martínez L F, Flores-Camacho J M, Balderas-Navarro R E, Chavira-Rodríguez M, Lastras-Martínez A and Cardona M 2007 *Phys. Rev.* B **75** 235315
[30] Mochán W L, Récamier J, Monsivais G and Diaz-Barriga L 1992 Photons low energy particles in surface processing *Fall 1991 Materials Research Society Symp. Proc.* vol 236, ed C Ashby, J H Brannon and S Pang (Pittsburgh: MRS) p 511
[31] Born M 1914 *Ann. Phys., Lpz.* **44** 605
[32] Pérez-Rodríguez F, Récamier J and Mochán W L 1998 *Surf. Sci.* **414** 93
[33] Keating P N 1966 *Phys. Rev.* **145** 637
[34] Pérez-Sánchez F L and Pérez-Rodríguez F 2004 *Phys. Status Solidi* c **1** 3065
[35] Weber W 1974 *Phys. Rev. Lett.* **33** 371
[36] Weber W 1977 *Phys. Rev.* B **15** 4789
[37] Tütüncü H M, Jenkins S J and Srivastava G P 1997 *Phys. Rev.* B **56** 4656
[38] Kress C, Fiedler M, Schmidt W G and Bechstedt F 1994 *Phys. Rev.* B **50** 17697
[39] Krüger P and Pollmann J 1995 *Phys. Rev. Lett.* **74** 1155
[40] Scholze A, Schmidt W G and Bechstedt F 1996 *Thin Solid Films* **281/282** 256
[41] Steckel J A, Kresse G and Hafner J 2002 *Phys. Rev.* B **66** 155406
[42] Palummo M, Pulci O, Marini A, Reining L and Del Sole R 2006 *Phys. Rev.* B **74** 235431
[43] Gavrilenko V I and Shkrebtii A I 1995 *Surf. Sci.* **324** 226
[44] Gavrilenko V I and Bechstedt F 1997 *Phys. Rev.* B **56** 3903
[45] Kress C, Shkrebtii A and Del Sole R 1997 *Surf. Sci.* **377–379** 398
[46] Palummo M, Pulci O, Del Sole R, Marini A, Schwitters M, Haines S R, Williams K H, Martin D S, Weightman P and Butler J E 2005 *Phys. Rev. Lett.* **94** 087404
[47] Tütüncü H M, Bağcı S and Srivastava G P 2004 *Phys. Rev.* B **70** 195401

[48] Thachepan S, Okuyama H, Aruga T, Nishijima M, Ando T, Bağcı S, Tütüncü H M and Srivastava G P 2003 *Phys. Rev.* B **68** 033310
[49] Alfonso D R, Drabold D A and Ulloa S E 1995 *Phys. Rev.* B **51** 1989
[50] Alfonso D R, Drabold D A and Ulloa S E 1995 *Phys. Rev.* B **51** 14669
[51] Warren J L, Yarnell J L, Dolling G and Cowley R A 1967 *Phys. Rev.* **158** 805
[52] Mahan G D and Obermair G 1969 *Phys. Rev.* **183** 834
[53] Dub P 1981 *Phys. Status Solidi* b **183** 109
[54] Lee S T and Apai G 1993 *Phys. Rev.* B **48** 2684
[55] Pehrsson P E and Mercer T W 2000 *Surf. Sci.* **460** 49
[56] Pérez-Sánchez F L and Pérez-Rodríguez F unpublished